Photodissociation dynamics of the phenyl radical via photofragment translational spectroscopy

Bogdan Negru, Scott J. Goncher,[a] Amy L. Brunsvold,[b] Gabriel M. P. Just, Dayoung Park, and Daniel M. Neumark[c]

Department of Chemistry, University of California, Berkeley, California 94720, USA and Chemical Sciences Division, Lawrence Berkeley National Laboratory, Berkeley, California 94720, USA

(Received 28 May 2010; accepted 12 July 2010; published online 16 August 2010)

Photofragment translational spectroscopy was used to study the photodissociation dynamics of the phenyl radical C_6H_5 at 248 and 193 nm. At 248 nm, the only dissociation products observed were from H atom loss, attributed primarily to $H+o\text{-}C_6H_4$ (*ortho*-benzyne). The observed translational energy distribution was consistent with statistical decay on the ground state surface. At 193 nm, dissociation to $H+C_6H_4$ and $C_4H_3+C_2H_2$ was observed. The C_6H_4 fragment can be either $o\text{-}C_6H_4$ or $l\text{-}C_6H_4$ resulting from decyclization of the phenyl ring. The $C_4H_3+C_2H_2$ products dominate over the two H loss channels. Attempts to reproduce the observed branching ratio by assuming ground state dynamics were unsuccessful. However, these calculations assumed that the C_4H_3 fragment was $n\text{-}C_4H_3$, and better agreement would be expected if the lower energy $i\text{-}C_4H_3+C_2H_2$ channel were included. © *2010 American Institute of Physics*. [doi:10.1063/1.3473743]

I. INTRODUCTION

The phenyl radical $c\text{-}C_6H_5$ plays a central role in the combustion chemistry of aromatic hydrocarbons. Its formation from the bimolecular reaction of smaller aliphatic species has been proposed to be the rate-limiting step in the production of larger aromatic molecules.[1,2] During combustion, the phenyl radical can undergo oxidation to form phenyl peroxy and phenoxy radicals.[3] Phenyl can also polymerize to form polycyclic aromatic hydrocarbons,[4] or it can decompose. The phenyl peroxy radicals are very reactive species that can further react with other hydrocarbons, while polycyclic aromatic hydrocarbons can further polymerize and lead to soot formation. The phenyl radical is an intermediate in the thermal decomposition of benzene,[5] so its bimolecular reactivity and unimolecular decay kinetics are of considerable interest in formulating a complete mechanism for this process. These considerations motivate the work described herein, in which the collisionless photodissociation decay dynamics of phenyl are investigated using photofragment translational spectroscopy.

Interest in the phenyl radical as a combustion intermediate dates back to the shock-tube study by Bauer[5] in 1963, where phenyl was observed as an intermediate in the thermal decomposition of benzene. Subsequent shock-tube studies on benzene decomposition[6,7] confirmed the role of phenyl as an intermediate. Collisionless photodissociation studies of benzene at 193 nm showed phenyl to be the major photoproduct.[8]

Solution phase kinetics of the phenyl radical with multiple substrates were examined by Scaiano and Stewart.[9] Gas phase bimolecular reactions of phenyl with various hydrocarbons have been investigated in a series of kinetics experiments by Lin and co-workers,[10–12] in which phenyl radicals were produced by pulsed laser photolysis and rate constants were determined by mass spectrometry and cavity ring-down spectroscopy. Cavity ring-down spectroscopy was also used by Tonokura *et al.*[13] to investigate phenyl radical reactions with Cl, O_2, and Cl_2. Kaiser and co-workers[14,15] carried out more detailed dynamics studies of phenyl bimolecular chemistry in a series of crossed molecular beam experiments where product kinetic energy and angular distributions were determined.

The spectroscopy of the phenyl radical has been investigated in several laboratories. The ultraviolet absorption spectrum of phenyl was measured in the gas phase by Ikeda *et al.*[16] and in an Ar matrix by Radziszewski.[17] The resulting electronic bands have been assigned and simulated in theoretical work.[18,19] The high resolution infrared spectrum of phenyl was reported by Sharp *et al.*[20] The photoelectron spectra of the phenyl radical[21,22] and phenide anion[23] have yielded the ionization potential and electron affinity of phenyl, while Sveum *et al.*[24] determined its photoionization cross section. The geometry, vibrational frequencies, and electron affinity of phenyl have also been investigated with electronic structure calculations.[25]

The work described in this paper is motivated by previous theoretical and experimental studies of the unimolecular decay of the phenyl radical. The relevant potential energy diagram, adapted from a calculation by Madden *et al.*,[26] is shown in Fig. 1 and shows three low-lying decay channels,

$$c\text{-}C_6H_5 \rightarrow o\text{-}C_6H_4 + H \quad \Delta H_0 = 76.0 \text{ kcal/mol}, \tag{1}$$

$$c\text{-}C_6H_5 \rightarrow l\text{-}C_6H_5 \rightarrow n\text{-}C_4H_3 + C_2H_2 \quad \Delta H_0 = 98.2 \text{ kcal/mol}, \tag{2}$$

[a]Present address: Department of Chemistry, Columbia University, New York, New York 10027, USA.
[b]Present address: SINTEF Energiforskning, Trondheim, Norway.
[c]Author to whom correspondence should be addressed. Electronic mail: dneumark@berkeley.edu.

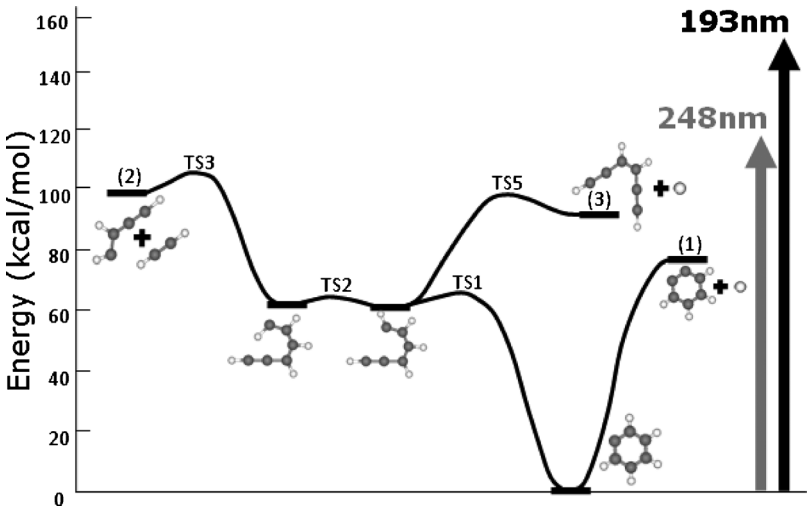

FIG. 1. Potential energy surface for the phenyl radical as calculated by Madden *et al.* (Ref. 26) at the G2M level of theory. The asymptotic channels 1, 2, and 3 are indicated.

$$c\text{-}C_6H_5 \rightarrow l\text{-}C_6H_5 \rightarrow l\text{-}C_6H_4 + H$$
$$\Delta H_0 = 91.0 \text{ kcal/mol}. \quad (3)$$

These energetics are very similar to those reported recently by Lories *et al.*[27]

Channel 1, the lowest energy channel, involves simple C–H bond fission to form *ortho*-benzyne, whereas channels 2 and 3 involve ring opening as the reaction proceeds over TS1 (decyclization) followed by either C–C or C–H bond fission. Early theoretical work[28,29] on phenyl radical formation and dissociation focused only on channel 2 and did not consider H atom loss via channel 1. Experiments performed on the pyrolysis of benzene and chlorobenzene[30] were interpreted in the context of these earlier studies; the H atom signal observed in this work was attributed to further dissociation of the C_4H_3 fragment produced by channel 2. However, theoretical work by Madden *et al.*[26] and Wang *et al.*[31] questioned these conclusions, since the earlier studies did not take into account that both fragmentation barriers for linear C_6H_5, depicted in Fig. 1, are higher in energy than the recyclization barrier, and that the energy required for $o\text{-}C_6H_5+H$ formation is substantially smaller than for $n\text{-}C_4H_3+C_2H_2$ formation. These calculations raise the issue of the competition between H+*o*-benzyne, which can occur via simple C–H bond fission, with the two decay channels that ensue upon decyclization. Rate constants as a function of energy calculated by Madden indicate that H+*o*-benzyne dominates at low energy, but that the other channels become progressively more important with increasing energy. Work by Wang indicated that tighter transition states for H atom loss than that used by Madden are needed to model shock-tube data. Experiments by Tseng and co-workers[32] found that 10% of the phenyl radicals formed from the photodissociation of C_6H_5NO at 193 nm further decomposed into H+benzyne, thus providing direct evidence for the importance of this channel.

In order to more directly address the above issues regarding unimolecular decay of the phenyl radical, we have investigated the collisionless decomposition dynamics of the phenyl radical using photofragment translational spectroscopy[33] at 248 and 193 nm in order to characterize the primary photochemistry of phenyl. Following the assignments of Kim *et al.*,[18] excitation at 248 nm accesses the $1\ ^2B_2$ and $3\ ^2A_1$ states via π-π^* transitions, while at 193 nm, the $2\ ^2B_2$ state is accessed by a stronger π-n transition, populating the σ orbital at the site of the missing H atom in phenyl. At 248 nm, only H atom loss was observed, but at 193 nm, channel 2 was also seen and, somewhat unexpectedly, was found to dominate over H atom loss.

II. EXPERIMENTAL

The work presented here was performed on a molecular beam photodissociation apparatus with a fixed source and a rotatable detector in which photodissociation products were analyzed with electron impact ionization mass spectrometry. Details of our detection scheme are sketched in Fig. 2 and have been described previously.[34,35] Phenyl radicals were produced with a newly built flash pyrolysis source following the design of Kohn *et al.*[36] A piezoactivated valve was used to produce a pulsed nitrosobenzene (C_6H_5NO) beam seeded in helium. A mixture of 0.2% C_6H_5NO was obtained by flowing 4 atm of He over a solid sample of nitrosobenzene at room temperature and applying 1 atm of this mixture to the pulsed valve with a vacuum regulator. The phenyl radical beam was generated via pyrolysis of the nitrosobenzene beam within a resistively heated SiC tube. This pyrolytic source is shown in Fig. 2 and consists of a SiC tube supported by a pair of molybdenum electrodes that are attached to the pulsed valve by a water-cooled copper block and an electrically insulating alumina spacer.

The phenyl radical beam was collimated by two skimmers that separated the source chamber from the main chamber. Within the main chamber, the radical beam was crossed at 90° with the 2×4 mm^2 focused beam spot of the photodissociation laser. Pulse energies of 40 mJ were obtained from a GAM excimer laser at 248 nm or a Lambda-Physik excimer laser at 193 nm. The scattered photofragments were detected as a function of laboratory angle Θ in the plane defined by the molecular beam and laser beam. After entering the triply differentially pumped detector, the neutral photofragments were ionized by electron impact, mass selected with a quadrupole mass filter, and detected with a Daly style ion detector. The acquired time of flight (TOF) spectra con-

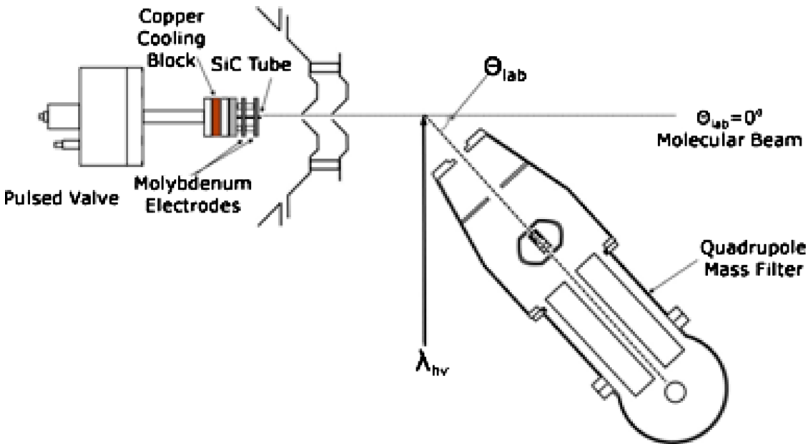

FIG. 2. Schematic of apparatus showing the radical source, photodissociation laser, and rotating mass spectrometer detector.

sisted of ion counts as a function of time and were obtained using a multichannel scaler interfaced to a computer. Each spectrum shown was accumulated over 300–500 thousand laser shots at a laser repetition rate of 100 Hz. The pulsed valve, however, was operated at 200 Hz so that background subtraction could be performed. An iterative forward convolution method was used to simulate the TOF spectra and thus determine the photofragment translational energy distributions in the center-of-mass frame of reference.

The radical beam was characterized using a spinning, retractable slotted chopper disk. Beam velocities were typically ~2200 m/s. The speed ratio, defined as the ratio between the beam flow velocity and velocity spread, was in the range of 4–6. Mass spectra of the molecular beam taken with the SiC tube unheated and subsequently heated to a temperature of about 1700 °C are shown in Fig. 3. There is significant dissociative ionization (DI) induced by electron impact ionization. Signal at $m/z=77$ corresponding to $C_6H_5^+$ was seen even from the unheated source, presumably from DI of nitrosobenzene. The phenyl photodissociation experiments were conducted by passing the minimum current through the SiC tube needed to eliminate fully the nitrosobenzene parent ion signal at $m/z=107$. Under these operating conditions, the $m/z=77$ signal in the bottom figure should be from the phenyl radical; this assumption was tested experimentally as discussed in Sec. III.

III. RESULTS

TOF spectra were taken for $m/z=76$ ($C_6H_4^+$), $m/z=51$ ($C_4H_3^+$), and $m/z=26$ ($C_2H_2^+$), the ionized primary fragments for channels (1)–(3), and for several of the daughter ions formed by dissociative ionization in the electron impact ionizer. Figure 4 shows the TOF spectra of the $m/z=76$ signal obtained from 248 and 193 nm photodissociation collected at laboratory scattering angles Θ ranging from 3° to 8°. Figure 5 shows the TOF spectra for the $m/z=51$ and $m/z=26$ photofragments at $\Theta=9°-15°$. Figure 6 shows the TOF spectra taken at 193 nm for $\Theta=6°-8°$ at $m/z=50$; these spectra were used to obtain product branching ratios as described in Sec. IV. In these figures, the TOF data are represented with open circles, while simulations obtained via forward convolution (see Sec. IV) are represented with solid lines. All spectra are background-subtracted as described above. TOF spectra were not collected for $m/z=1$ owing to kinematic factors that cause this signal to be very low, along with high background at this mass-to-charge ratio.

Fragments with $m/z=76$ were observed at both photodissociation wavelengths but only over a very narrow range of laboratory scattering angles near the molecular beam. The observed angular range is larger at 193 nm, reflecting more translational energy release at the higher photon energy. This signal was also more intense at 193 nm than at 248 nm, consistent with the larger phenyl absorption cross section at 193 nm.[17] TOF signal for the lighter masses ($m/z=51,26$) was considerably weaker, and signal at angles $\Theta \geq 9°$ was seen only at 193 nm.

The raw TOF data suggest the presence of H atom loss at both wavelengths and channel 2 at 193 nm only, but several

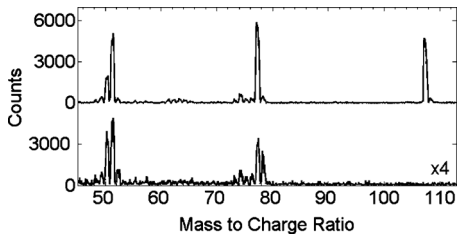

FIG. 3. Mass spectra of the molecular beam of nitrosobenzene in helium taken with the pyrolytic source unheated in the upper trace and heated in the lower trace.

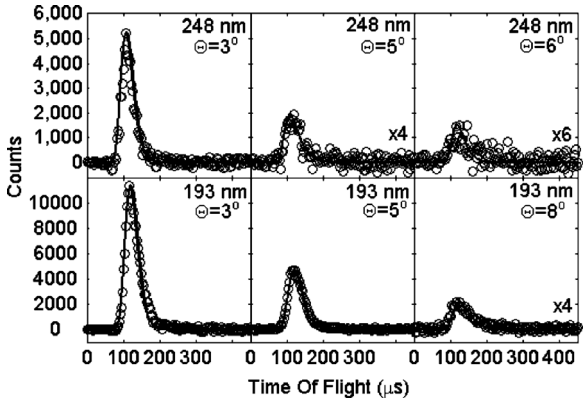

FIG. 4. Characteristic TOF spectra for $m/z=76$ ($C_6H_4^+$) fragments collected at $\Theta_{lab}=3°$, 5°, 6°, and 8° obtained from 248 and 193 nm photodissociation of c-C_6H_5. The fits to these TOF spectra (solid lines) are generated from the $P(E_T)$ distributions in Figs. 8 and 9, respectively.

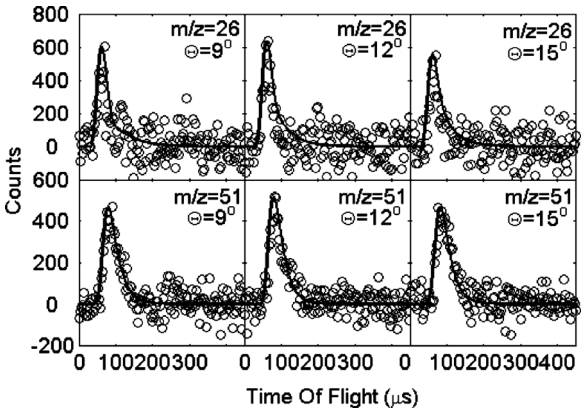

FIG. 5. Characteristic TOF spectra for $m/z=51$ ($C_4H_3^+$) and $m/z=26$ ($C_2H_2^+$) fragments collected at $\Theta_{lab}=9°$, 12°, and 15° obtained from 193 nm photodissociation of c-C_6H_5. A single $P(E_T)$ distribution, shown in Fig. 10, was used to fit these spectra.

checks are required to confirm this assignment. For example, a possible concern in this experiment is that photodissociation of any benzene or nitrosobenzene in the beam will produce C_6H_5 and C_6H_4 photofragments, thereby interfering with C_6H_4 photofragments created from phenyl photodissociation. Nitrosobenzene photodissociation studies[32] at both 248 and 193 nm show the presence of only one dissociation channel, the production of C_6H_5 and NO. To check for this channel, we looked for photodissociation signal at $m/z=77$ ($C_6H_5^+$). These spectra did not show distinguishable signal at 248 or 193 nm, consistent with complete decomposition of the parent compound in the pyrolysis source. At 193 nm, the major benzene photodissociation channel is phenyl+H.[8] The absence of signal at $m/z=77$ rules out contamination from benzene at this wavelength. At 248 nm, benzene dissociates to $C_6H_4+H_2$, which could interfere with the $m/z=76$ signal from phenyl photodissociation. To check for this, TOF data were simulated with the previously published translational energy distribution for this channel.[8] This procedure yielded significantly faster C_6H_4 photoproducts than were seen in our experiment. Hence, we can rule out interference from benzene at both wavelengths.

The assignment of the TOF features to phenyl dissociation must also be consistent with the photodissociation kinematics, as outlined in the Newton diagram in Fig. 7 for 193 nm excitation. Each circle represents the maximum speed in the center-of-mass frame for the detected fragments produced from radical photodissociation. From the measured

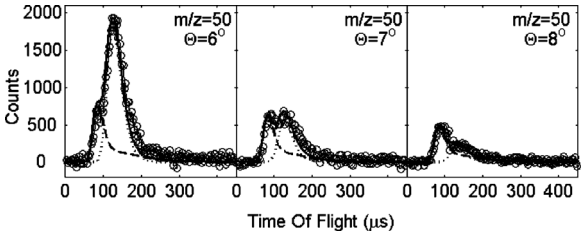

FIG. 6. TOF spectra of $m/z=50$ ($C_4H_2^+$) at 193 nm showing contributions from daughter ions of mass 76 and mass 51 fragments. In each spectrum, these contributions are fit, respectively, with a dotted line using the $P(E_T)$ distribution in Fig. 9 and a dashed line using the $P(E_T)$ distribution in Fig. 10. The solid black line shows the sum of the dashed and dotted simulations.

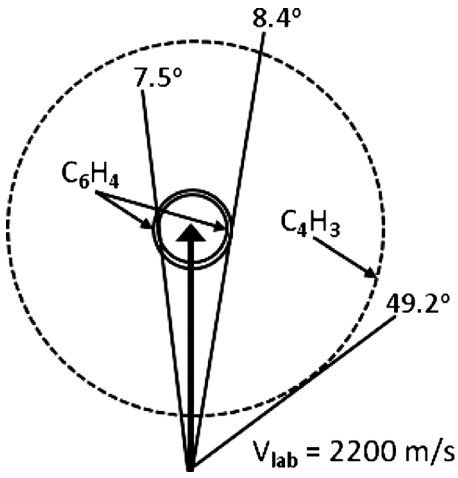

FIG. 7. Newton diagram for the phenyl radical photodissociation at 193 nm. Each circle represents the maximum center-of-mass speeds of product photofragments. The solid black circles represent the C_6H_4 fragments, while the dotted circle represents the n-C_4H_3 fragment. Maximum laboratory scattering angles for the fragments are shown.

phenyl beam velocity, the maximum laboratory angle for a particular channel can then be determined from the diagram. The solid black circles correspond to C_6H_4 fragments from channel 1 and channel 3; the small diameter of these circles reflects the large mass ratio of the fragments for these channels (76:1) and results in a very restricted range of laboratory angles over which C_6H_4 product can be observed from phenyl dissociation. The fact that the experimental TOF signal for $m/z=76$ ions falls within these limits here as well as within the corresponding limits at 248 nm supports our attribution of this signal to phenyl photodissociation.

The dotted black circle in Fig. 7 represents the C_4H_3 product from channel 2 at 193 nm; the corresponding circle for its C_2H_2 counterpart is much larger and is not shown. The Newton circles for both products are considerably larger than that for C_6H_4. As a result, these fragments can be observed over a larger spread of laboratory angles, consistent with the data in Fig. 5. These kinematic considerations rule out dissociative ionization of C_6H_4 as the source of the signal at $m/z=51$ and 26 in Fig. 5, since the laboratory angles at which these data were taken lie below the maximum laboratory scattering angle of C_6H_4.The other key kinematic consideration is that if the $m/z=51$ and 26 signals come from phenyl dissociation, they should be "momentum-matched," i.e., their TOF distributions should be reproduced from the same center-of-mass translational energy distribution. This point is considered further in Sec. IV.

IV. ANALYSIS

The above results show that at least two phenyl photodissociation channels are present: H atom loss at both wavelengths and, at 193 nm, an additional channel involving fragmentation to two heavy fragments. Center-of-mass photofragment energy and angular distributions $P(E_T, \theta)$ for each of these reaction channels were obtained by fitting the TOF spectra of the photodissociated fragments. The $P(E_T, \theta)$

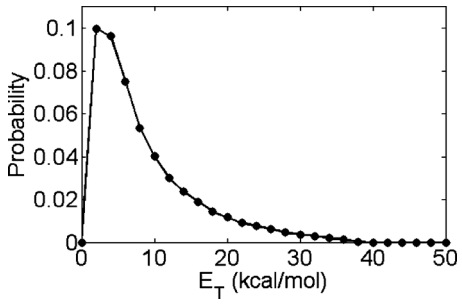

FIG. 8. Center-of-mass $P(E_T)$ distribution from phenyl photodissociation at 248 nm to $H+C_6H_4$. The maximum available translational energy assumed for channel 1 is set at 37 kcal/mol. Due to the minimum laboratory detection angle of 3° for the current experimental setup, points below 5 kcal/mol are less reliable than those at higher energy.

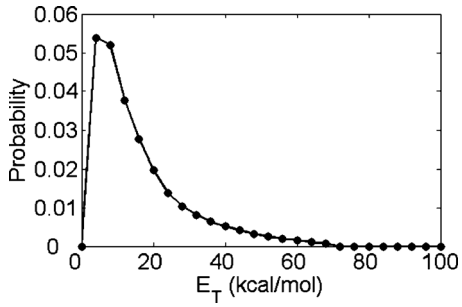

FIG. 9. Center-of-mass $P(E_T)$ distribution from phenyl photodissociation at 193 nm to form $H+C_6H_4$. The maximum available translational energy assumed for channel 1 is set at 72 kcal/mol. Due to the minimum laboratory detection angle of 3° for the current experimental setup, points below 5 kcal/mol are less reliable than those at higher energy.

distribution can be rewritten in terms of the uncoupled center-of-mass translational energy $P(E_T)$ and angular distribution $I(\theta,E_T)$,

$$P(E_T,\theta) = P(E_T)I(\theta,E_T). \tag{4}$$

In our experimental geometry, where the rotational axis of the detector is normal to the plane defined by the molecular and laser beams, an anisotropic angular distribution is possible even with unpolarized excimer laser beams, but a satisfactory fit to the data was obtained assuming an isotropic distribution for all values of E_T. The PHOTRAN (Ref. 37) forward convolution program was used to simulate TOF spectra for all the data sets according to an assumed $P(E_T)$ distribution. The input $P(E_T)$ distribution for a channel was adjusted point-wise until a best fit was simultaneously obtained for all the TOF spectra of that channel. By conservation of energy, the total center-of-mass translational energy E_T is given by

$$E_T = h\upsilon + E_0 - E_{\text{int}} - D_0. \tag{5}$$

Here $h\upsilon$ is the photon energy, D_0 is the dissociation energy for the channel of interest [from Eqs. (1)–(3)], E_{int} is the total internal energy of the fragments, and E_0 is the initial energy of the phenyl radicals. The maximum translational energy for a particular channel for cold radicals (E_0=0) is given by $h\upsilon - D_0$.

The best fits obtained for the H loss channel at 248 nm are superimposed on the TOF spectra from Fig. 4. The $P(E_T)$ distribution in Fig. 8 used to simulate these TOF spectra peaks close to 0 kcal/mol, with an average translational energy $\langle E_T\rangle$=9 kcal/mol, and extends to 37 kcal/mol, the maximum translational energy available for channel 1. The $P(E_T)$ distribution that fits the H loss channel from 193 nm photodissociation is shown in Fig. 9. The corresponding TOF simulations are superimposed on the data in Fig. 4. For this distribution, $\langle E_T\rangle$=16 kcal/mol. It also extends to the maximum allowed translational energy for channel 1, 72 kcal/mol, otherwise its overall form is similar to that in Fig. 8. Note that channel 3 can contribute to H atom loss at both wavelengths; this channel would result in slower products that would be difficult to distinguish from channel 1. However, if we attempted to simulate the TOF spectra at either wavelength with a $P(E_T)$ distribution that extended only to the maximum energy allowed for channel 3, i.e., 22 kcal/mol at 248 nm and 57 kcal/mol at 193 nm, the fit was noticeably poorer near the largest scattering angles where signal at m/z=76 was observed.

The TOF spectra in Fig. 5 for m/z=51 and 26 can be fit with the $P(E_T)$ distribution shown in Fig. 10; the simulated TOF spectra are superimposed on the data in Fig. 5. Since the TOF spectra for the two ion masses are reproduced with only a single $P(E_T)$ distribution, these spectra are assigned to momentum-matched C_4H_3 and C_2H_2 photofragments from phenyl dissociation at 193 nm. The $P(E_T)$ distribution in Fig. 10 peaks at 8 kcal/mol with an average translational energy of $\langle E_T\rangle$=13 kcal/mol, and extends to 50 kcal/mol, the maximum allowed translational energy at this dissociation wavelength.

All TOF spectra at 248 nm were fit with the $P(E_T)$ distribution in Fig. 8, while those at 193 nm were fit using one or, in the case of Fig. 6, both of the $P(E_T)$ distributions in Figs. 9 and 10. Hence, there is no evidence for any primary photoproducts other than those associated with H atom loss and channel 2.

The universal detection scheme used in this experiment enables extraction of the following branching ratio at 193 nm,

$$\frac{\text{channel 2}}{\text{channel}(1+3)} = R \times \frac{\sigma_{C_6H_4}}{\sigma_{C_4H_3}} \times \frac{f_{C_6H_4}}{f_{C_4H_3}}. \tag{6}$$

The ratio R represents the relative weights of the $P(E_T)$ distributions used by the fitting program to reproduce the rela-

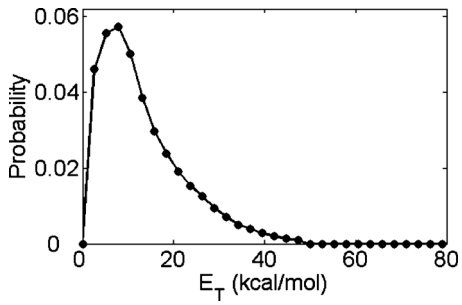

FIG. 10. Center-of-mass $P(E_T)$ distribution for the $C_4H_3+C_2H_2$ channel shown in Fig. 6. This distribution was used to fit the TOF spectra for both m/z=51 and 26. The maximum allowed translational energy is set at 50 kcal/mol.

tive intensities of contributions of H atom loss and channel 2 to the TOF spectra shown in Fig. 6. The values of σ denote the relative electron impact cross sections of the C_6H_4 and C_4H_3 photofragments determined by the additivity scheme of Fitch and Sauter,[38] while f is the fraction of signal for the indicated species appearing at $m/z=50$ via dissociative ionization. These fractions, 56% for C_6H_4 and 43% for C_4H_3, were determined by taking TOF spectra at $\Theta=4°$ and 12° at all values of m/z that yielded measurable photodissociation signal ($m/z=76$, 75, 74, 73, 61, 60, 51, 50, 49, 48, 37, and 36). The channel 2/channel(1+3) branching ratio was thus found to be 5.3 ± 0.8; estimated error bars are from Schmoltner.[39]

V. DISCUSSION

The main objectives of this study were to (a) determine the primary photochemistry of the phenyl radical and (b) to gain insight into the overall photodissociation mechanism. The key mechanistic question is whether dissociation occurs on one or more excited state surfaces or by internal conversion to the ground state followed by statistical decay. This issue can be addressed by considering the translational and angular energy distributions of the various product channels as well as the product branching ratios, and determining if these attributes are consistent with statistical decay on the ground state surface.

The unimolecular decomposition pathways of the phenyl radical on its ground state as determined by the electronic structure calculations by Madden *et al.*[26] are shown in Fig. 1. On this surface, the lowest energy dissociation channel, channel 1, proceeds via C–H bond cleavage with no exit barrier. The higher energy channels 2 and 3 involve decyclization of phenyl via TS1 and dissociation over TS3 and TS5, respectively; the calculated barrier heights of TS3 and TS5 with respect to the associated product channels are 7.4 and 6.0 kcal/mol. If dissociation does occur on the ground state surface, one would expect channel 1 to dominate at low excitation energies, while channels 2 and 3 would become progressively more important at higher excitation energies. Moreover, based on the calculated topography of the ground state surface, ground state dissociation would result in a $P(E_T)$ distribution for channel 1 peaking at very low E_T, while the distributions for channels 2 and 3 would peak at higher kinetic energies owing to the small exit barriers for both channels.

These expectations are largely borne out by the experimental data. At 248 nm, only H atom loss is observed. The $P(E_T)$ distribution for this channel peaks below 5 kcal/mol; C_6H_4 fragments with lower kinetic energy cannot be seen below the minimum laboratory scattering angle (3°) at which we can collect data. In contrast, in the photodissociation of comparably sized polyatomic molecules that undergo H atom loss on an excited state surface, the kinetic energy distributions peak much closer to the maximum allowed value.[40] Overall, the $P(E_T)$ distribution in Fig. 8 and the associated isotropic angular distribution are consistent with ground state dissociation. Assuming this to be the case, then elementary considerations of statistical unimolecular decay would predict that channel 1 will dominate at this wavelength, even though channel 3 is accessible and cannot be easily distinguished from channel 1 in our data. We have performed a more quantitative analysis of the branching between channels 1 and 3 using the microcanonical rate constants reported by Madden *et al.*[26] and indeed find this to be the case, with channel 1 accounting for over 90% of the products. Hence, at 248 nm, simple C–H bond fission to form H+*o*-benzyne is the dominant dissociation mechanism.

At 193 nm, phenyl dissociates via H atom loss and by channel 2, with channel 2 as the dominant pathway. The $P(E_T)$ distribution for H atom loss is similar to that at 248 nm, except that it extends to higher E_T and, as a consequence, $\langle E_T \rangle$ is higher. The $P(E_T)$ distribution for channel 2 peaks around 8 kcal/mol. As was the case at 248 nm, all data could be fit assuming an isotropic angular distribution. The $P(E_T)$ distribution for channel 2 is consistent with ground state dissociation over the small exit barrier (TS3) on the surface shown in Fig. 1. Under these circumstances, one would expect the H atom loss channel at 193 nm to have significant contributions from channels 1 and 3, because once decyclization of the phenyl radical occurs, channel 3 should occur in addition to channel 2.

One must also consider the product branching ratios in evaluating the dissociation mechanism at 193 nm. We find the channel 2/channel (1+3) ratio to be 5.3 ± 0.8. For ground state dissociation, this value implies that (a) decyclization dominates over C–H bond fission to generate H+*o*-benzyne, and that (b) once decyclization does occur, channel 2 dominates over channel 3. Both results are rather surprising, at first glance. Channel 1 is not only lower in energy than the two decyclization channels but also, according to Fig. 1, proceeds without an exit barrier, in contrast to channels 2 and 3. Under these circumstances, one would expect a larger unimolecular rate constant for a low energy channel that proceeds by a loose transition state compared to a higher energy channel involving a tight transition state. Moreover, it is not obvious by inspection of Fig. 1 why channel 2 should prevail over channel 3.

These questions can be addressed by considering the variational Rice–Ramsperger–Kassel–Marcus calculations by Madden *et al.*,[26] in which microcanonical rate constants as a function of energy were calculated for C–H bond fission (channel 1), decyclization (over TS1), recyclization (the reverse reaction over TS1), and dissociation of the decyclized intermediate to channels 2 and 3. These calculations showed that the transition state for channel 1 is not as loose as, for example, the transition state for the $H+CH_3$ recombination reaction [r(C–H)=3.4 Å at T=300 K],[41] and that it moved inward along the reaction coordinate with increasing internal energy, thereby reducing the rate constant for channel 1. Specifically, the value of r(C–H) that produced the smallest rate constant for channel 1 dropped from 2.9 Å at 300 K to 2.3 Å at 2500 K. In addition, although TS5 leading to channel 3 is lower in energy than TS3 leading to channel 2, the rate constant for dissociation over TS3 becomes larger at a total energy of 150 kcal/mol, presumably reflecting the larger number of available states at TS3 with increasing energy.

Using the microcanonical rate constants from Madden *et*

al. with r(C–H)=2.3 Å for the channel 1 transition state, we calculated the product branching ratios by solving their kinetic model. We found that by 155 kcal/mol total energy, which is comparable to the energy of a 193 nm photon (148 kcal/mol), channel 2 was larger than either channel 1 or channel 3, and that as the energy was further increased, so did the relative contribution from channel 2. However, the channel 2 yield did not equal the sum of channels 1 and 3 until considerably higher energy (190 kcal/mol), and did not approach the experimental branching ratio under any circumstances. It thus appears that the experimental product branching ratio is not consistent with statistical unimolecular decay on the potential energy surface in Fig. 1, suggesting either that the surface needs to be improved, or that nonstatistical dynamics are at play at 193 nm.

In fact, the surface in Fig. 1 is incomplete as it only considers the n-C_4H_3+C_2H_2 channel and does not include i-C_4H_3+C_2H_2. Two recent high-level electronic structure calculations[42,43] find that i-C_4H_3 (H_2CCCCH) lies 12 kcal/mol lower in energy than n-C_4H_3 (HCC(H)CCH). Moreover, calculations by Lories *et al.*[27] find that the exit barrier for dissociation to i-C_4H_3+C_2H_2 is 7.9 kcal/mol. These values, when applied to Fig. 1, result in a transition state lying at 94.1 kcal/mol with respect to the bottom of the C_6H_5 well, lower than either TS3 (105.6 kcal/mol) or TS5 (97.0 kcal/mol). While additional hydrogen-shifting is required to reach i-C_4H_3+C_2H_2 from phenyl, Lories *et al.* find the barriers for these processes to be considerably lower than the exit barrier, indicating that dissociation of energized phenyl to i-C_4H_3+C_2H_2 is feasible. The implications of this new pathway for our experiment are significant, as it represents a channel that would compete more effectively with both channels 1 and 3 on the ground state surface. In particular, the lower exit barrier relative to TS5 would drop the yield of channel 3 substantially. Hence, while rate constants for dissociation to i-C_4H_3+C_2H_2 have not been reported to date, inclusion of this channel in an overall kinetic model would clearly produce better agreement with our experimental branching ratio at 193 nm.

VI. CONCLUSIONS

The photodissociation dynamics of the phenyl radical have been explored at 248 and 193 nm using photofragment translational spectroscopy. Translational energy $P(E_T)$ distributions and product branching ratios were determined. At 248 nm, only H+C_6H_4 products were observed. The $P(E_T)$ distribution indicated a reaction coordinate with little or no barrier, and this channel was attributed primarily to H+o-C_6H_4 (channel 1) formed by C–H bond fission on the ground state surface.

At 193 nm, H atom loss was observed along with momentum-matched C_4H_3+C_2H_2 products. The $P(E_T)$ distributions for H atom loss again peaked at very low energy, while that for C_4H_3+C_2H_2 (channel 2) peaked around 8 kcal/mol, consistent with dissociation over a small exit barrier. This channel results from decyclization of the phenyl radical prior to dissociation. The decyclized radical can also dissociate to H+l-C_6H_4 (channel 3), so this channel along with the lower energy channel 1 can contribute to the overall dissociation via H atom loss at 193 nm. The branching ratio, channel 2/channel (1+3), was 5.3 ± 0.8. The kinetic energy distributions for the two mass channels were suggestive of ground state dissociation dynamics. However, using microcanonical rate constants previously determined by Madden *et al.*, we were unable to reproduce the experimental branching ratio, finding too little channel 2. These calculations, however, assumed that channel 2 was n-C_4H_3+C_2H_2, and we would expect that incorporation of the lower energy i-C_4H_3+C_2H_2 channel into the overall kinetics would result in considerably better agreement with experiment.

ACKNOWLEDGMENTS

This work was supported by the Director, Office of Basic Energy Sciences, Chemical Sciences Division of the U.S. Department of Energy under Contract No. DE-AC02-05CH11231. The authors also thank Ralf Kaiser and Stephen Klippenstein for helpful discussions.

[1] M. Frenklach, Phys. Chem. Chem. Phys. **4**, 2028 (2002).
[2] H. Richter and J. B. Howard, Phys. Chem. Chem. Phys. **4**, 2038 (2002).
[3] I. V. Tokmakov, G. S. Kim, V. V. Kislov, A. M. Mebel, and M. C. Lin, J. Phys. Chem. A **109**, 6114 (2005).
[4] M. Shukla, A. Susa, A. Miyoshi, and M. Koshi, J. Phys. Chem. A **112**, 2362 (2008).
[5] S. H. Bauer and C. F. Aten, J. Chem. Phys. **39**, 1253 (1963).
[6] M. Braun-Unkhoff, P. Frank, and T. Just, Proc. Combust. Inst. **22**, 8 (1988).
[7] A. Laskin and A. Lifshitz, Proc. Combust. Inst. **26**, 6 (1996).
[8] A. Yokoyama, X. Zhao, E. J. Hintsa, R. E. Continetti, and Y. T. Lee, J. Chem. Phys. **92**, 4222 (1990).
[9] J. C. Scaiano and L. C. Stewart, J. Am. Chem. Soc. **105**, 3609 (1983).
[10] T. Yu and M. C. Lin, J. Phys. Chem. **99**, 8599 (1995).
[11] I. V. Tokmakov, J. Park, and M. C. Lin, ChemPhysChem **6**, 2075 (2005).
[12] J. Park, G. J. Nam, I. V. Tokmakov, and M. C. Lin, J. Phys. Chem. A **110**, 8729 (2006).
[13] K. Tonokura, Y. Norikane, M. Koshi, Y. Nakano, S. Nakamichi, M. Goto, S. Hashimoto, M. Kawasaki, M. P. S. Andersen, M. D. Hurley, and T. J. Wallington, J. Phys. Chem. A **106**, 5908 (2002).
[14] R. I. Kaiser, L. Vereecken, J. Peeters, H. F. Bettinger, P. V. Schleyer, and H. F. Schaefer, Astron. Astrophys. **406**, 385 (2003).
[15] X. B. Gu and R. I. Kaiser, Acc. Chem. Res. **42**, 290 (2009).
[16] N. Ikeda, N. Nakashima, and K. Yoshihara, J. Am. Chem. Soc. **107**, 3381 (1985).
[17] J. G. Radziszewski, Chem. Phys. Lett. **301**, 565 (1999).
[18] G. S. Kim, A. M. Mebel, and S. H. Lin, Chem. Phys. Lett. **361**, 421 (2002).
[19] M. Biczysko, J. Bloino, and V. Barone, Chem. Phys. Lett. **471**, 143 (2009).
[20] E. N. Sharp, M. A. Roberts, and D. J. Nesbitt, Phys. Chem. Chem. Phys. **10**, 6592 (2008).
[21] V. Butcher, M. L. Costa, J. M. Dyke, A. R. Ellis, and A. Morris, Chem. Phys. **115**, 261 (1987).
[22] J. Hrušak, D. Schroder, and S. Iwata, J. Chem. Phys. **106**, 7541 (1997).
[23] R. F. Gunion, M. K. Gilles, M. L. Polak, and W. C. Lineberger, Int. J. Mass Spectrom. Ion Process. **117**, 601 (1992).
[24] N. E. Sveum, S. J. Goncher, and D. M. Neumark, Phys. Chem. Chem. Phys. **8**, 592 (2006).
[25] J. C. Rienstra-Kiracofe, D. E. Graham, and H. F. Schaefer, Mol. Phys. **94**, 767 (1998).
[26] L. K. Madden, L. V. Moskaleva, S. Kristyan, and M. C. Lin, J. Phys. Chem. A **101**, 6790 (1997).
[27] X. Lories, J. Vandooren, and D. Peeters, Phys. Chem. Chem. Phys. **12**, 3762 (2010).
[28] M. J. S. Dewar, W. C. Gardiner, M. Frenklach, and I. Oref, J. Am. Chem. Soc. **109**, 4456 (1987).
[29] S. P. Walch, J. Chem. Phys. **103**, 8544 (1995).
[30] V. S. Rao and G. B. Skinner, J. Phys. Chem. **92**, 2442 (1988).

[31] H. Wang, A. Laskin, N. W. Moriarty, and M. Frenklach, Proc. Combust. Inst. **28**, 1545 (2000).
[32] C. M. Tseng, Y. M. Choi, C. L. Huang, C. K. Ni, Y. T. Lee, and M. C. Lin, J. Phys. Chem. A **108**, 7928 (2004).
[33] L. J. Butler and D. M. Neumark, J. Phys. Chem. **100**, 12801 (1996).
[34] Y. T. Lee, J. D. McDonald, P. R. Lebreton, and D. R. Herschbach, Rev. Sci. Instrum. **40**, 1402 (1969).
[35] J. C. Robinson, S. A. Harris, W. Z. Sun, N. E. Sveum, and D. M. Neumark, J. Am. Chem. Soc. **124**, 10211 (2002).
[36] D. W. Kohn, H. Clauberg, and P. Chen, Rev. Sci. Instrum. **63**, 4003 (1992).
[37] S. A. Harich, PHOTRAN (2003).
[38] W. L. Fitch and A. D. Sauter, Anal. Chem. **55**, 832 (1983).
[39] A. M. Schmoltner, Ph.D. thesis, University of California, Berkeley, 1989.
[40] M. N. R. Ashfold, G. A. King, D. Murdock, M. G. D. Nix, T. A. A. Oliver, and A. G. Sage, Phys. Chem. Chem. Phys. **12**, 1218 (2010).
[41] W. L. Hase, S. L. Mondro, R. J. Duchovic, and D. M. Hirst, J. Am. Chem. Soc. **109**, 2916 (1987).
[42] S. E. Wheeler, W. D. Allen, and H. F. Schaefer, J. Chem. Phys. **121**, 8800 (2004).
[43] S. J. Klippenstein and J. A. Miller, J. Phys. Chem. A **109**, 4285 (2005).